Chapter 9
A Power Flow Control Scheme for a Photovoltaic to a Low Voltage Microgrid System

S Z Sayed Hassen, M I Jahmeerbacus, K Sewraj and M S Ruhomaun

Department of Electrical and Electronic Engineering

University of Mauritius

{z.sayedhassen@uom.ac.mu; iqbal@uom.ac.mu; keshav.sewraj@umail.uom.ac.mu; sameer070892@gmail.com}

Abstract The increasing penetration of renewable energy sources into the ac grid has brought several challenges for the power utilities, especially in the fields of power quality, stability, reliability, protection and control. In this paper, we present the design and implementation of a power flow control scheme for a photovoltaic to low voltage ac grid interface. The control algorithm is based on instantaneous tracking of the power reference signal by current regulation of the grid connected inverter. The proposed control and graphical user interface are implemented using LabVIEW. The ability of the developed system to control both the real and reactive powers injected into the grid is validated using both computer simulations and experimental tests.

Keywords: Photovoltaic, Microgrid, Power Control.

9.1 Introduction

Distributed Generation (DG) typically includes photovoltaic panels, wind turbines and waste-to-energy sources, among others. Although renewable energy sources are environmental friendly compared to fossil fuels, they also come with a set of challenges for the power utilities, namely in the areas of power quality, harmonics, stability, protection and control. Moreover, massive deployment of distributed generation may affect key grid parameters such as line frequency and voltage, and calls for a coordinated approach for integrating DG in the network.

Microgrids can operate in both grid-connected and islanded mode [1], where generators and loads are usually interconnected at low voltage. On the utility side, a connected microgrid can be controlled as if it were one entity. Islanded microgrids however have characteristics which are quite different, compared to those of the conventional power system. In grids powered by synchronous generators, unbalances

between the generated power and electrical power consumption are compensated by the inertia of the rotating system, resulting in a change of frequency. Non-mechanical energy sources, such as photovoltaic arrays, are however interfaced to the microgrid through power electronic converters [2], [3]. The control of both active and reactive powers by such converters enables better frequency and voltage regulation.

In this paper, we propose the design and implementation of a power flow control scheme between a photovoltaic array with battery energy storage and a low voltage microgrid. The control algorithms and graphical user interfaces are developed using LabVIEW to regulate power transfer from the dc side to the ac grid. The paper is organized as follows: Section 9.2 describes the main stages and modeling of the microgrid system, including the photovoltaic panel, and the power flow control from battery to grid through an inverter. Section 9.3 presents the main simulation and experimental results for power flow control between the dc side and the ac grid, with injection of real and reactive power at varying phase. A typical charging performance of the energy storage battery is also demonstrated. Section 9.4 finally provides some concluding remarks.

9.2 Modeling, control and design of proposed system

A block diagram describing the proposed setup is shown in Fig. 9.1. Variations in solar irradiance affect both the current-voltage characteristics and the output power of the photovoltaic (PV) array. The battery bank is charged from the PV array with maximum power tracking operation and provides energy storage at a stable terminal voltage. The dc to ac inverter converts the battery output dc voltage to ac while matching the power and frequency requirements of the microgrid.

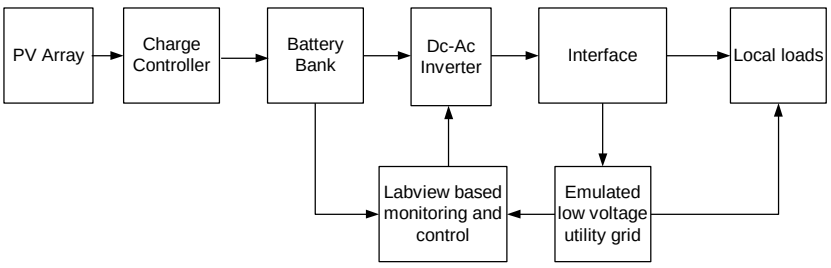

Fig. 9.1. Block diagram of proposed system

9.2.1 Modeling and Characteristics of PV array

The equivalent circuit model of a PV cell is shown in Fig. 9.2, where I_{ph} and D are an ideal current source and diode, respectively. The non-ideal cell characteristics are represented by the insertion of resistors R_s and R_p [4]. The generated current (I_{ph}) depends on the solar irradiance (S) and the temperature T so that:

$$I_{ph} = (I_{sc} + k_i(T - T_r))\left(\frac{S}{1000}\right) \tag{9.1}$$

where I_{sc} is a reference short-circuit current, T_r a reference temperature, and k_i the short-circuit temperature coefficient.

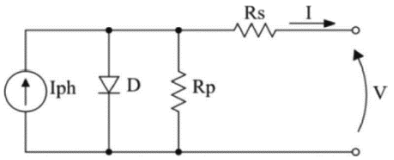

Fig. 9.2. Equivalent Model of a PV cell [4]

The PV panel simulation model is represented by

$$I = I_{ph} - I_r\left[e^{\frac{q(V+IR_s)}{\eta kT}} - 1\right] - \frac{V + IR_s}{R_p} \tag{9.2}$$

where V is the output voltage of one PV panel, I_{ph} is the photocurrent, I_r is the saturation current, q is the electronic charge, η is the p-n junction quality factor, k is the Boltzmann's constant and T is the panel temperature.

A 75 W BP275F PV module [5], [6] is used to implement the photovoltaic source. The current-voltage and the power-voltage characteristics of the PV module are generated using Eqs. (9.1) and (9.2), as shown in Figs. 9.3 and 9.4, respectively. The PV panel is specified at an operating temperature of 25 ^{0}C. However, due to panel exposure to direct sunlight and dusty environment for extended times, the actual power output is to be adjusted according to the ambient temperature and dust reduction factors [8], [9], respectively.

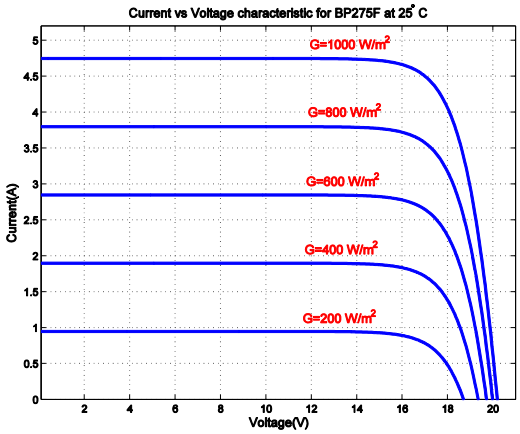

Fig. 9.3. Current-voltage characteristics of PV panel

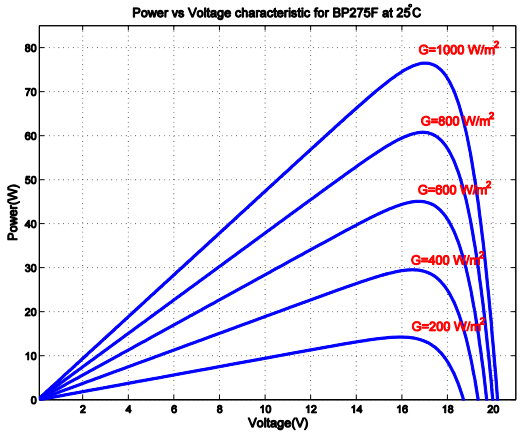

Fig. 9.4. Power-voltage characteristics with varying solar irradiance

The charging process of the lead-acid battery bank consists of a bulk stage at constant current and rising voltage, an absorption stage at constant voltage with falling current, and a float stage. As solar irradiance varies, the charge controller adjusts the instantaneous voltage and current to the battery, according to the charging mode.

9.2.3 Interface Between Dc Side and Low Voltage Ac Grid

The power conversion stage from the dc to low voltage grid interface is shown in Fig. 9.5. At a given time instant, power can be transferred from battery to the grid, or vice-versa. However, the cycle average real power transferred to the grid is positive. Transformer T provides electrical isolation between the single phase mains and the inverter output, and also steps down the mains voltage to v_g.

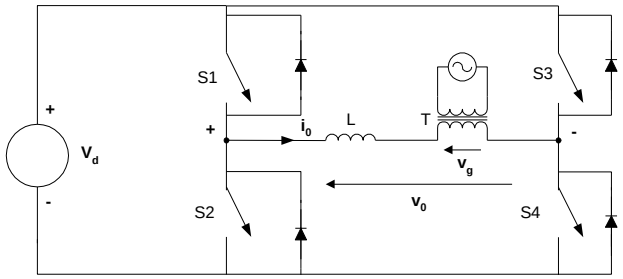

Fig. 9.5. Dc to low-voltage ac side interface through switch-mode inverter

The power semiconductor switches, S1 to S4, are controlled to track a sinusoidal reference current at a predefined phase angle, and to deliver the target real power to the grid. Since the inverter switches are operated in either the on or off states, the output voltage and current contain harmonics at the switching frequency and its multiples. The harmonic content in the output current therefore needs to be minimized to improve the power quality of the inverter to grid interface. Tracking of sinusoidal current is achieved by a hysteresis band current controller. The ac side inductor caters for the voltage difference between the inverter output and the grid voltage and also helps to filter out the high frequency harmonics in the injected current.

9.2.4 Power control into ac side

It is required to control the active and reactive components of the power between the inverter and the ac grid. Hence the PV-inverter combination can be configured to operate at unity power factor, or as a reactive power source with leading or lagging power factors.

The instantaneous power due to the fundamental components of the injected current (i_1) and utility voltage (v_g) at grid frequency (f_1) can be expressed as

$$p(\theta) = v_g(\theta) i_1(\theta) \tag{9.3}$$

where:

$$v_g(\theta) = V_m \sin\theta \tag{9.4}$$

$$i_1(\theta) = I_m \sin(\theta - \phi) \tag{9.5}$$

$$\theta = 2\pi f_1 t \tag{9.6}$$

ϕ is the phase lag of the injected current with respect to the grid voltage.

From Eq. (9.3), the average real power is given by

$$P = S\cos\phi \tag{9.7}$$

where S is the apparent power and is expressed as:

$$S = \frac{V_m I_m}{2} \tag{9.8}$$

The power flow control scheme is represented in Fig. 9.6. The signal *e(k)* represents the error between the reference and actual powers at the k^{th} sampling instant. The Proportional + Integral (PI) controller output, *u(k)*, represents the amplitude of the current to be injected into the grid. This control signal is multiplied by a sinusoidal template and applied to a hysteresis band controller to generate the switching signals of the dc to ac inverter.

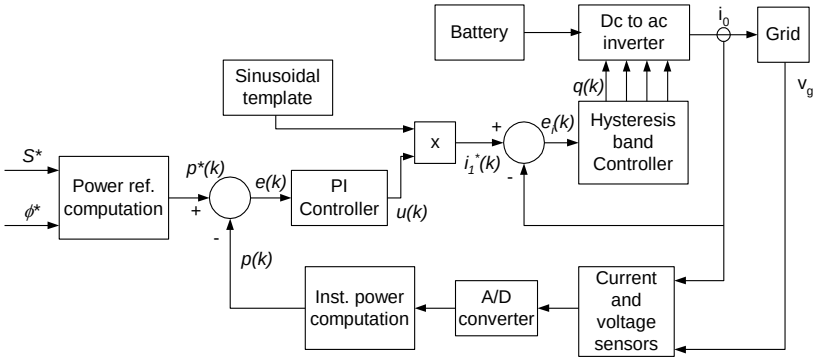

Fig. 9.6. Block diagram of proposed power controller

9.2.4.1 Reference and actual instantaneous powers, and PI power controller

The power to be injected into grid can be described by the apparent power command (S^*), and the phase angle (ϕ^*) between injected current and grid voltage. From Eqs. (9.3) to (9.6), the instantaneous power reference can be expressed as:

$$p^*(k) = S^*\left[\cos\phi^*(k) - \cos(4\pi f_1 kT_s - \phi^*(k))\right] \tag{9.9}$$

where T_s is the sampling time period.

To obtain the actual instantaneous power injected, voltage and current sensors are incorporated in the ac line. After appropriate signal conditioning and sampling of the measured signals v_g and i_0, the instantaneous power is computed as:

$$p(k) = v_g(k) i_0(k) \tag{9.10}$$

The PI controller outputs the required amplitude of the grid-injected current, so that:

$$u(k) = K_e e(k) + (K_i T_s - K_e) e(k-1) + u(k-1) \tag{9.11}$$

where K_e and K_i are the proportional and integral gains respectively, and

$$e(k) = p^*(k) - p(k) \tag{9.12}$$

9.2.4.2 Hysteresis band current controller

To adjust the real and apparent powers, the required phase shift of the inverter output current is described by Eq. (9.5). The reference current, $i_1^*(k)$, is obtained using the output signal from the PI controller. Hence:

$$i_1^*(k) = u(k)\sin[2\pi f_1 kT_s - \phi^*(k)] \tag{9.13}$$

where ϕ^* is the phase shift command.

The hysteresis band controller generates switching signals q_1 to q_4 for the inverter power transistors S1 to S4, respectively, as shown in Fig. 9.7. Signal $e_i(k)$ represents the error between the reference and actual line currents, and is given by:

$$e_i(k) = i^*(k) - i_0(k) \tag{9.14}$$

The hysteresis band controller output signals are given by:

$$q_1(k) = q_4(k) = \begin{cases} 1 & e_i(k) > h \\ 0 & e_i(k) < h \\ q_1(k-1) & otherwise \end{cases} \tag{9.15}$$

and

$$q_2(k) = q_3(k) = \bar{q}_1(k) \tag{9.16}$$

where h is the width of the hysteresis band.

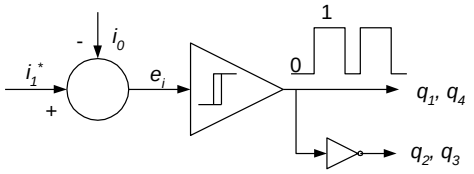

Fig. 9.7. Generation of inverter switching signals

9.3. Simulation and experimental tests

To investigate the effectiveness of the proposed power control scheme, an experimental test bed with graphical user interface was implemented. The main parameters of the system under test are summarized in Table 9.1.

Table 9.1. Parameters of the battery to inverter to grid link

Parameter	Value
Injected power rating	20 VA
Power factor	0 (lagging/ leading) to 1
Ac side voltage and frequency	7 V (rms), 50 Hz
Battery bank nominal voltage	24 V
Inverter output side inductance	5 mH

The main components of the test setup are shown in Fig. 9.8. A National Instruments NI RIO GPIC inverter controller card [6], [7] implements the control algorithm described in Section 9.2 and supplies the switching signals to the dc to ac inverter. The same board acquires the measured ac side signals through Hall-effect current and voltage sensors. The control software and graphical user interface are implemented with LabVIEW graphical programming for FPGA.

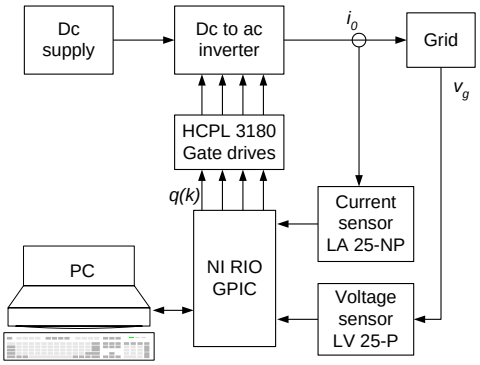

Fig. 9.8. Main components of the implemented system

9.3.1 Battery charging profile

Fig. 9.9 shows the charging profile of the battery over a test interval of 85 minutes. The bulk charging stage maintains a fairly constant current of about 2 A while the charging voltage rises gradually from 22 V to 26 V. In the absorption stage the charging current falls below 1.4 A, while the voltage remains between 25 V to 26 V.

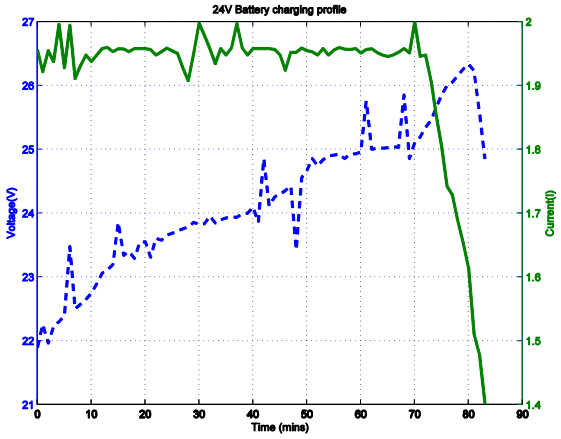

Fig. 9.9. Battery charging profile (solid line: current, dotted line: voltage)

9.3.2 Power control from inverter to grid

The power control scheme described in Section 9.2 is validated through computer simulations and experimental results. The inverter and controller models are built using Simulink^{TM} software, and tested for different power commands. The response plots are compared with the corresponding experimental results for power factors of unity and zero (leading), respectively.

9.3.2.1 Operation at unity power factor

Fig. 9.10 shows the response plots for the grid voltage and current when the injected power command is at 10 VA, unity power factor. The simulation and experimental results are in close agreement, showing the zero phase shift between injected current and grid voltage. The total harmonic distortion in the inverter output current is 4.2 %.

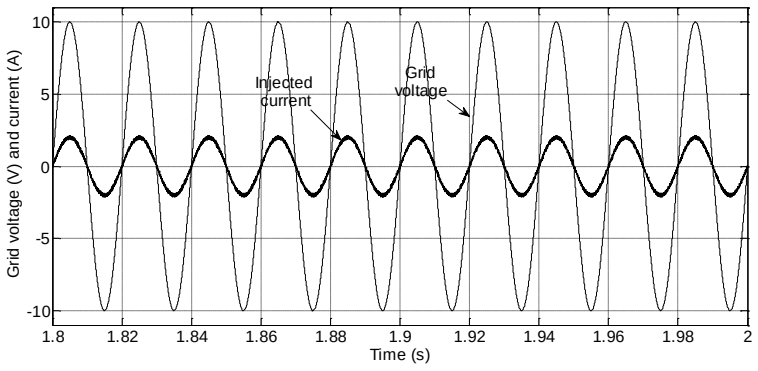

(a)

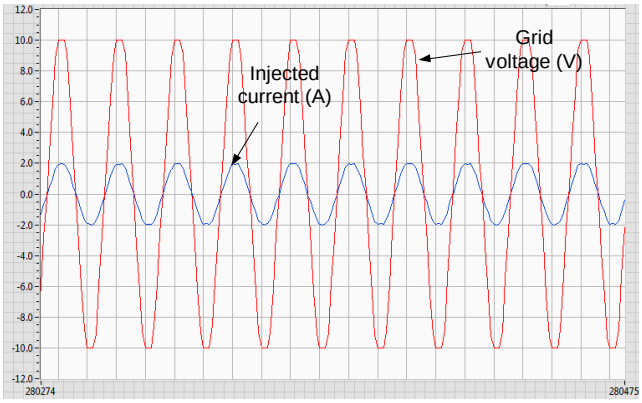

(b)

Fig. 9.10. **(a)** Simulation and **(b)** Experimental results for i_0 and v_g at S = 10 VA, cos ϕ = 1

The instantaneous power variations between the dc and ac sides are shown in Figs 9.11(a) and (b). Since the injected power has no reactive component, the power flow is always positive and has an average value of 10 W, corresponding to the command value.

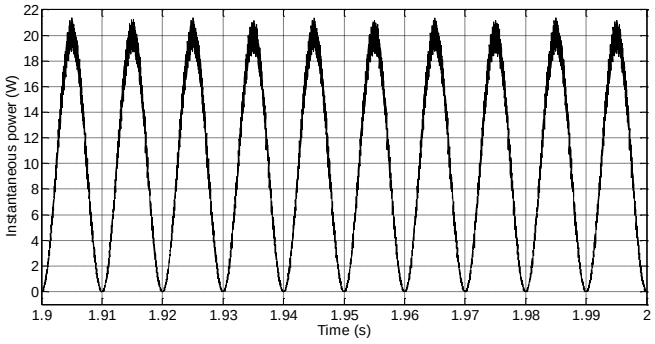

(a)

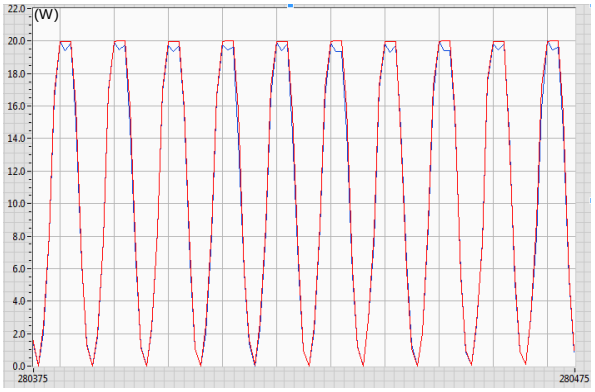

(b)

Fig. 9.11. (a) Simulation and **(b)** Experimental results for instantaneous power at cos ϕ = 1

9.3.2.2 Operation at zero power factor, leading

The power command is next adjusted to inject purely reactive power (leading) into the ac side. The corresponding simulation and experimental results are shown in Figs. 9.12 and 9.13. The inverter output current is seen to lead the grid voltage by 90^0. As a result, the instantaneous power response has zero average value and the reactive power is 9.5 VAr.

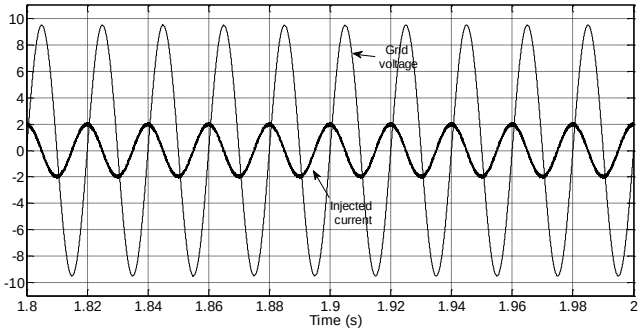

Fig. 9.12. (a) Simulation results for i_0 and v_g at S = 9.5 VA, cos ϕ = 0 (lead)

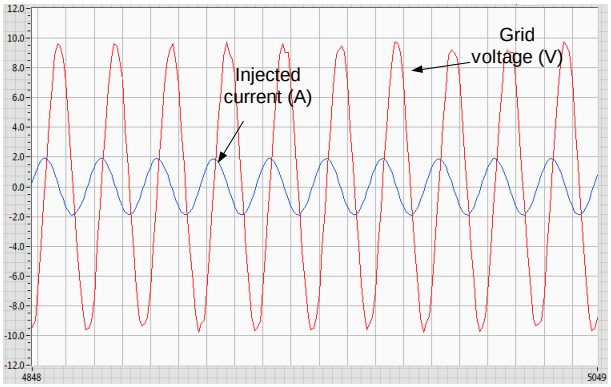

Fig. 9.12. (b) Experimental results for i_0 and v_g at S = 9.5 VA, cos ϕ = 0 (lead)

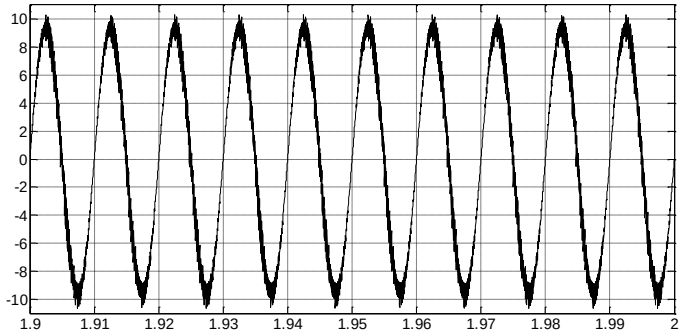

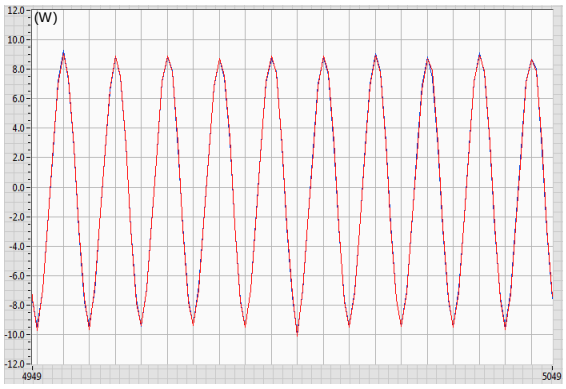

Fig. 9.13. (a) Simulation and **(b)** Experimental results for instantaneous power, cos ϕ = 0 (lead)

9.4. Conclusion

The modeling and design of a power flow control scheme from a photovoltaic array to low voltage ac grid have been presented. The proposed method is based on generating the output current command for the switch-mode dc to ac inverter, based on the error between the reference and actual instantaneous powers. A current tracking scheme using hysteresis band control ensures that the inverter output current has the required amplitude and phase shift with respect to the grid voltage. The implemented system has been tested under various power commands, including purely real and purely reactive power injection. In all cases, the instantaneous power responses closely follow the reference profiles, and the injected currents into the ac side are nearly sinusoidal with low harmonic distortion.

Acknowledgments. The authors wish to thank the University of Mauritius for funding this research work (No. R182), and for all the facilities provided.

References

1. Vandoorn, T. L., et al., “Microgrids – Hierarchical control and an Overview of the Control and Reserve Management Strategies”, IEEE Ind. Electronics Magazine, Vol. 7, No. 4, pp. 42-55, Dec. 2013.
2. Serban, I. ; Teodorescu, R. ; Marinescu, C.: “Analysis and optimization of the battery energy storage systems for frequency control in autonomous microgrids, by means of hardware-in-the-loop simulations" 3rd IEEE International Symposium on Power Electronics for Distributed Generation Systems (PEDG, pp. 374 - 379), 2012.
3. Poh Chiang Loh ; Ding Li ; Blaabjerg, F.:"Autonomous control of interlinking converters in hybrid AC-DC microgrids with energy storages" Energy Conversion Congress and Exposition (ECCE), pp.652 - 658, 2011.
4. Gomes De Brito, M.A., et al., “Evaluation Of The Main MPPT Techniques For Photovoltaic Applications” IEEE Trans. On Industrial Electronics, Vol. 60, No. 3, March 2013, pp. 1156-1167
5. Ruhomaun, M.S., "Solar charge controller with maximum power point tracking", B.Eng. (Hons) dissertation, University of Mauritius, 2015.
6. Sayed Hassen, S.Z., Jahmeerbacus, M.I, Sewraj, K., and Ruhomaun, M.S., "Development and Control of an Experimental Test Bed for a Microgrid Using LabVIEW", Internally funded project, University of Mauritius, 2015.
7. Sewraj, K., "Control of microgrid-connected dc to ac inverter with LabView interface", B.Eng. (Hons) dissertation, University of Mauritius, 2015.
8. Zorilla, J., *et al.*, "Analysis of dust losses in photovoltaic modules", Proc. World Energy Congress, May 2011, pp. 2985-2992.
9. Rashid, M. (ed.), "Power Electronics Handbook", 3rd edition, Elsevier Inc., 2011.